A Study of the Adsorption Properties of Single Walled Carbon Nanotubes Treated with Nitric Acid†

Andrés A. García Blanco[1], Jhonny Villarroel Rocha[1], John F. Múnera[2], Marcelo Nazzarro[1], Giorgio Zgrablich[1] and Karim Sapag[1*] *(1) Instituto de Física Aplicada, CONICET-Universidad Nacional de San Luis, Chacabuco 917, San Luis, C.P. 5700, Argentina. (2) Instituto de Investigaciones en Catálisis y Petroquímica, FIQ, CONICET-Universidad Nacional del Litoral, Santa Fe, Argentina.*

(Received 1 May 2011; accepted 22 July 2011)

ABSTRACT: The changes observed in the properties of Single Walled Carbon Nanotubes (SWCNTs) after treatment with nitric acid are reported. The oxidized nanotube samples were characterized morphologically by scanning electron microscopy and structurally by Raman spectroscopy, thermogravimetric analysis, infrared spectroscopy and X-ray photoelectron spectroscopy. Gas adsorption was used to study the changes in the surface properties of the samples (including the changes in their porosity), as well as the changes in the adsorbate–adsorbent interactions which occurred as a result of the acid treatment. The adsorption studies were conducted using nitrogen at 77 K and CO_2 at different temperatures between 263 K and 289 K at sub-atmospheric pressures. The isosteric heat was calculated from the data obtained and indicated a higher adsorbate–adsorbent interaction for the oxidized materials. A correlation was found between morphological and structural evolution and the adsorption properties of CO_2, a probe gas which appears to be very suitable for characterizing the microporosity of these kinds of materials.

1. INTRODUCTION

Research into the properties and applications of carbon nanotubes has been very active ever since the first report of the existence of these materials by Iijima (1991). In recent years, numerous studies have reported significant results on the application of carbon nanotubes to electronic devices and sensors (Dai 2002; Baughman *et al*. 2002), to gas storage (Zhou *et al*. 2003; Dillon *et al*. 1997; Rzepka *et al*. 1998; Lee *et al*. 2000; Panella *et al*. 2005; Simonyan and Johnson 2002; Ansón *et al*. 2004; Kim *et al*. 2008; Cao *et al*. 2003; Lu *et al*. 2008) and to heterogeneous catalysis (Serp *et al*. 2003; Yin *et al*. 2004; Graham *et al*. 2009; Chen *et al*. 2008). Knowledge of the adsorption properties of carbon nanotubes is important for the development of nanotube-based materials for the aforementioned applications. Hence, there is considerable interest in attaining a detailed characterization of the adsorption properties of carbon nanotubes (Eswaramoorthy *et al*. 1999; Ohba and Kaneko 2002; Yang *et al*. 2002; Cinke *et al*. 2003; Migone and Talapatra 2004; Krungleviciute *et al*. 2004; Furmaniak *et al*. 2006; Rawat *et al*. 2008; Albesa *et al*. 2010; Cruz *et al*. 2010; Esteves *et al*. 2009).

Carbon nanotubes aggregate into cylindrical bundles in which the tubes are aligned along their long axis. One of the most important features of adsorption onto carbon nanotubes is the presence of

† Published in the Festschrift of the journal dedicated to Professor Giorgio Zgrablich on the occasion of his 70th birthday and to celebrate his 50 years as a faculty member at the National University of San Luis in Argentina.

*Author to whom all correspondence should be addressed. E-mail: sapag@unsl.edu.ar.

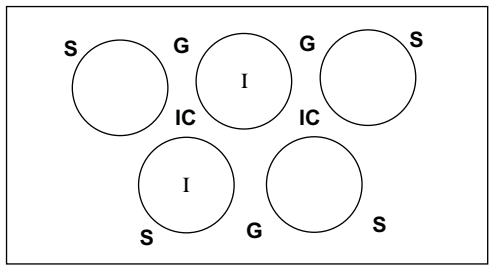

Figure 1. A cross-sectional view of the adsorption sites present in a SWCNT bundle: G, grooves; IC, interstitial channels; S, external surface of individual nanotubes; I, interior of the tubes.

different groups of adsorption sites (Krungleviciute *et al*. 2004; Albesa *et al*. 2010), which arise as a result of the aggregation of the nanotubes into bundles. These different sites give rise to the unique adsorption properties of nanotubes, such as the possibility of producing one-dimensional adsorbed phases, i.e. phases with high mobility in one direction and strongly restricted motion in the other two directions (Krungleviciute *et al*. 2004; Calbi *et al*. 2001; Talapatra and Migone 2001). There are three possible groups of adsorption sites for an array of closed nanotubes (see Figure 1): interstitial channels (IC), located between three neighbouring nanotubes; grooves (G), located at the junction between two neighbouring nanotubes on the outer surface of the bundle; and graphene layer sites (S) on the outer surface of individual nanotubes on the periphery of the bundles. For nanotubes with open ends, the interior of the nanotubes provides an additional group of adsorption sites (I) as shown in Figure 1.

All the currently known techniques for the production of SWCNTs generate significant amounts of carbonaceous impurities, such as amorphous carbon and carbon nanoparticles, often with a metal catalyst enclosed (Itkis *et al*. 2003). Acid purification is a useful process for removing the excess catalyst and amorphous carbon present in the as-produced nanotube samples. It is also an appropriate method for opening the ends of the nanotubes, since nanotubes are produced with closed ends (Kataura *et al*. 2000). In particular, nitric acid reflux is one of the most commonly used methods for the purification of SWCNTs. Previous studies have reported, however, that treatment with HNO_3 not only eliminates the catalyst, but also results in reactions with the carbon nanotubes themselves. In prolonged acid treatments, these reactions could destroy the SWCNTs (Hu *et al*. 2003).

The aim of the present study was to characterize the evolution of the adsorption properties of SWCNTs when they are subjected to oxidation treatment by refluxing in nitric acid. Attempts have been made to determine what changes in the structure of the material occur as a result of such treatment, and how these affect the adsorption properties. Scanning electron microscopy (SEM), thermogravimetric analysis (TGA), Raman spectroscopy (RS), Fourier-transform infrared spectroscopy (FT-IR) and X-ray photoelectron spectroscopy (XPS) have been used to characterize these materials. In addition, N_2 (at 77 K) and CO_2 (at 263, 273, 283 and 289 K) adsorption isotherms, at pressures between 2 Pa and 100 kPa, were performed.

2. EXPERIMENTAL

2.1. Sample preparation

In this work, experiments were conducted on single wall carbon nanotubes (labelled NT) produced by electric arc discharge and marketed by Carbon Solutions Inc. (sample characteristics are listed in Table 1). The oxidation studies were performed employing concentrated nitric acid

TABLE 1. SWCNT Characteristics as Provided by the Manufacturer

Carbonaceous purity[a]	60–70%
Metal content[b]	30%

[a]Determined according to the procedure described by Itkis *et al*. (2003).
[b]From thermogravimetric analysis in air.

(65 wt%) with the samples heated at 398 K in a reflux apparatus for 6, 10 and 14 h, respectively (these samples are labelled as NT6, NT10 and NT14, respectively, below). After allowing the nanotubes to cool, they were filtered using a cellulose acetate membrane (pore size, 0.22 μm) and washed with distilled water to a pH near 7.

2.2. Sample characterization

The morphology of the SWCNT samples was analyzed by SEM methods using a LEO 1450VP scanning electron microscope. Thermogravimetric analyses (TGA) were conducted on a Shimadzu TGA-50 instrument employing an air flow of 50 cm^3/min and a heating rate of 5 K/min from room temperature up to 1273 K.

Raman spectroscopy (RS) was employed to analyze the vibrational modes of the SWCNT samples. The Raman spectra were recorded using a LabRam spectrometer (Horiba-Jobin-Yvon) coupled to an Olympus confocal microscope (a 100× objective lens being used for simultaneous illumination and collection) equipped with a CCD detector cooled to ca. 200 K using the Peltier effect. The excitation wavelength was 532 nm in all cases (diode-pumped solid-state laser). The laser power was set at 30 mW. Integration times ranged from a few seconds to a few minutes, depending on the sample.

FT-IR spectroscopy was used to characterize the surface chemical groups present in the samples, using a Varian 640 IR apparatus equipped with an ATR camera for the determinations. X-Ray photoelectron spectroscopy (XPS) was used to characterize the evolution of the surface functional groups of the SWCNT samples. The X-ray photoelectron spectra were measured in a Vacuum Generation System Microtech ultra-high vacuum apparatus with an Al Kα radiation source at a pressure of 10^{-7} Pa. The binding energy was referred to the C1s peak at 284.5 eV.

Nitrogen (99.999%) adsorption/desorption isotherms at 77 K were measured on a Micromeritics ASAP 2000 instrument while CO_2 (99.996%) adsorption isotherms were measured on a Quantachrome Autosorb-1MP instrument, the temperature for each isotherm being controlled by a Cole Parmer Polystat temperature controller. The samples under study were degassed under vacuum conditions (0.5 Pa) for 12 h at 553 K before performing each adsorption isotherm. Calculations of the pore size distributions and micropore volumes were undertaken using the Non-Local Density Functional Theory (NLDFT) with the "N_2–carbon equilibrium transition at 77 K based on a cylindrical pore model" kernel (Autosorb-1 2.11 software – Quantachrome Instruments).

2.3. Characteristic curves

On the basis of Polanyi's theory of the adsorption potential (Polanyi 1914), Dubinin developed the theory of micropore volume filling to explain the adsorption of gases and vapours onto microporous adsorbents (Dubinin 1960). The Polanyi theory postulated that the attraction force at

any point in the adsorbed film could be expressed by the adsorption potential (A). This potential is thermodynamically equal to the free energy change of an adsorbate from the adsorbed phase to the bulk liquid phase (Wood 2001). The adsorption potential may be expressed as:

$$A = RT\ln\left(\frac{P_0}{P}\right) \tag{1}$$

The plot of the adsorbed volume, expressed as the liquid volume, as a function of the adsorption potential is called the "characteristic curve" (Dubinin 1960). Such curves at different temperatures for the same adsorbate should fall along the same curve. In addition, if the adsorption potential is corrected by an appropriate adsorbate affinity coefficient (β), the characteristic curves for different adsorbates should also fall along the same curve.

To obtain the characteristic curves of the adsorption of N_2 and CO_2, the following properties were determined:

(i) *The density of the adsorbed phase (ρ_s)*: For N_2 at 77 K, the adsorbed phase is considered as a saturated liquid; hence its density was estimated via the modified Rackett equation (Spencer and Danner 1972):

$$\frac{M}{\rho_s} = \left(\frac{RT_C}{P_C}\right)Z_{Ra}^{\left[1+(1-T/T_C)^{2/7}\right]} \tag{2}$$

where M is the molecular weight, T_C is the critical temperature, P_C is the critical pressure and Z_{Ra} is the Rackett compressibility factor [these values were taken from Reid *et al*. (1987)]. For CO_2, it is known that the density of the adsorbed phase is significantly higher than the density of the saturated liquid state (Garrido *et al*. 1987). Hence, the most accepted values of the adsorbed phase densities of CO_2 were considered, viz. 1.023 g/cm^3 at 273 K (Garrido *et al*. 1987; Rodríguez-Reinoso and Linares-Solano 1988) and 0.97 g/cm^3 at 298 K (Garrido *et al*. 1987). Taking account of the Dubinin consideration regarding the linear behaviour of the adsorbed phase density relative to temperature between the boiling point and the critical temperature (Dubinin 1960), it was possible to determine the densities at the other temperatures under study.

(ii) *Saturation pressure*: The CO_2 saturation pressures were estimated using the Wagner equation (Wagner 1973):

$$\ln\left(\frac{P_0}{P_C}\right) = \frac{AX + BX^{1.5} + CX^3 + DX^6}{1 - X}, \qquad X = 1 - \frac{T}{T_C} \tag{3}$$

where A, B, C and D are CO_2-specific constants as reported by Reid *et al*. (1987).

(iii) *Affinity coefficient*: The N_2 and CO_2 affinity coefficients were estimated employing the Vaskovsky equation (Dubinin 1960):

$$\beta = \frac{\Omega}{\Omega_{reference}} \tag{4}$$

where Ω and $\Omega_{reference}$ are the adsorbate and reference compound parachors, respectively. The most often used reference compound for carbonaceous materials is benzene. The parachors were calculated from Sugden atomic values (Quayle 1953).

2.4. Isosteric heat of adsorption

The isosteric heat of adsorption (q_{st}), defined as the enthalpy change before and after adsorption, provides a measure of the strength of interaction between adsorbate molecules and the adsorbent surface (Do 1998; Szekely *et al*. 1976). It is an important property for characterizing the type of adsorption taking place and the degree of heterogeneity of a surface (Satterfield 1993; Sircar 1991). The magnitude of the surface coverage and its dependence on the isosteric heat of adsorption provides useful information on the nature of the adsorbed phase. The isosteric heat of adsorption of a pure gas, for a fixed adsorbed amount, can be obtained from adsorption isotherms measured at different temperatures using the Clausius–Clapeyron equation (Ruthven 1984):

$$q_{st} = RT^2\left[\frac{\partial \ln P}{\partial T}\right]_V = -R\left[\frac{\partial \ln P}{\partial(1/T)}\right]_V \quad (5)$$

where R is the gas constant [8.314 J/(mol K)], P is the equilibrium pressure (kPa) for the pure gas at a temperature T (K) and V is the amount adsorbed (cm^3/g). This method is sensitive to errors in the adsorption isotherms (Dunne *et al*. 1996), so it is very important to make the correct choice of experimental isotherms for use in the calculation.

3. RESULTS

3.1. Sample characterization

3.1.1. SEM analysis

Figure 2 overleaf shows a sequence of SEM micrographs for the SWCNT samples (NT, NT6, NT10 and NT14) which display the evolution of the structure as a function of the acid-treatment time. Initially, the nanotubes had a disorganized tissue-like structure [Figure 2(a)] with many empty spaces between the bundles. Impurities — probably catalyst particles or amorphous carbon — can also be found in the untreated sample (NT). Figure 2(b) shows that the NT6 sample had denser regions and that its bundles appear more organized than in the NT sample, as reported by Yang *et al*. (2005) for an equivalent treatment. The characteristics of this sample were as if the tissue-like structure had been cut in some regions as a result of the acid treatment and condensed in others, showing a "brush-like" structure. Similar effects can be seen in the NT10 and NT14 samples [Figures 2(c) and (d), respectively], where the regions of condensation increased while the few individual bundles present grew in diameter.

3.1.2. Raman spectral analysis

Figure 3 overleaf displays the Raman spectra of the samples under study. A signal in the 100–400 cm^{-1} spectral region corresponds to the typical radial breathing mode (RBM) of the nanotubes. The RBM is a unique phonon mode which appears only in carbon nanotubes and its observation in the Raman spectrum provides direct evidence that a sample contains SWCNTs (Dresselhaus *et al*. 2005). The diameters of the nanotubes were calculated from these signals using the following equation (Lafi *et al*. 2005):

$$\omega = 238/d^{0.93} \quad (6)$$

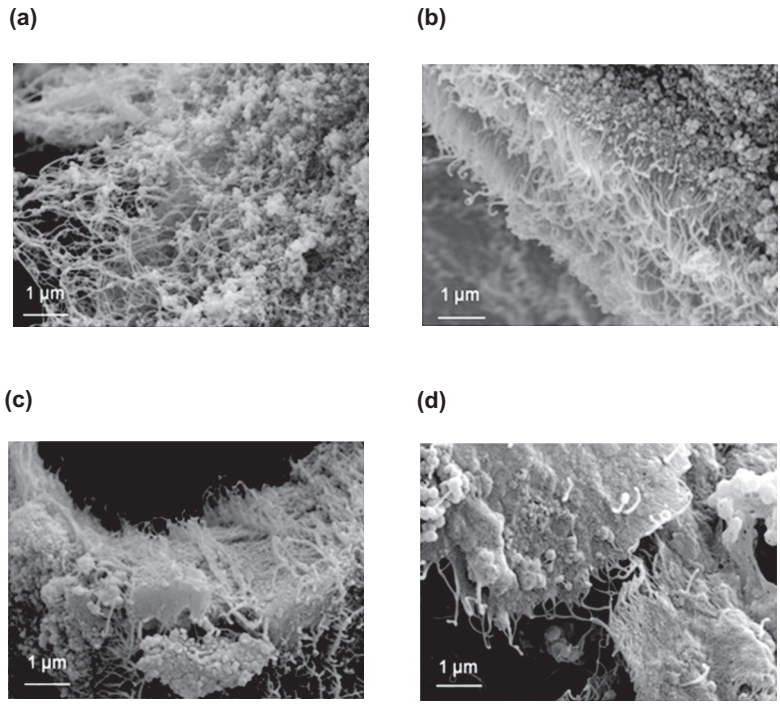

Figure 2. Scanning electron micrographs of the SWCNT samples studied, displaying the evolution of the SWCNT sample structure as a function of acid treatment: (a) NT; (b) NT6; (c) NT10; and (d) NT14.

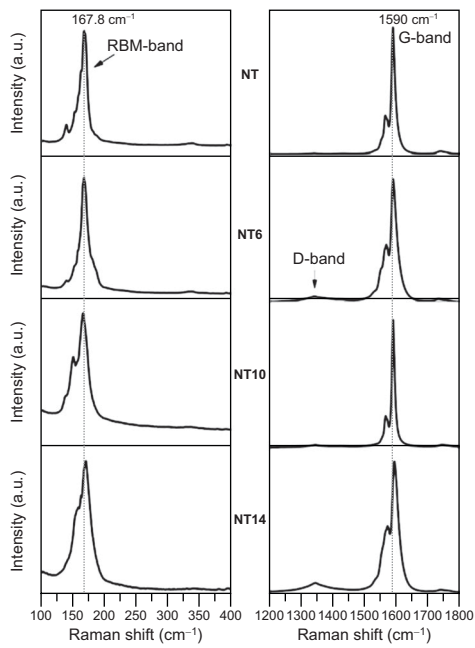

Figure 3. Raman spectra of the SWCNT samples studied.

where ω is the Raman shift (cm^{-1}) and d is the diameter (nm) of the nanotube, resulting in nanotube diameters between 1.5 nm and 1.8 nm. A relative increment in the amount of nanotubes with higher diameters occurred for acid-treatment times greater than 6 h (NT10 and NT14 samples).

The D-band intensity and the G-band width have both been considered as probes of SWCNT wall integrity or functionalization on the tube walls (Kim *et al*. 2005). The peaks corresponding to the tangential mode (TM) in the 1500–1650 cm^{-1} range, with the characteristic G-peak associated with the resonance of metallic and semiconducting SWCNTs (Lafi *et al*. 2005), are shown in Figure 3. The G-band at 1582 cm^{-1} is associated with graphite. For the SWCNTs, the peak at 1590 cm^{-1} may be related to in-plane vibrations along the tube axis, while the diameter-dependent G-peak at 1570 cm^{-1} is related to the in-plane vibrations along the circumferential direction. Both values are corroborated by the Raman spectral data results obtained by Dresselhaus *et al*. (2005).

Calculation of the intensity relations between the G-peak (at ca. 1590 cm^{-1}) and the peak corresponding to the RBM (at ca. 165 cm^{-1}), i.e. I_G/I_{RBM}, led to values of 3.6, 3.6, 7 and 6 for the NT, NT6, NT10 and NT14 samples, respectively. These results indicate that no destruction of the nanotubes in the as-produced sample occurred up to 6 h of treatment, whereas longer treatment times led to degradation of the sample. The higher intensity in the D-peak signal (at ca. 1340 cm^{-1}) for the NT14 sample indicates an increase in both the amounts of amorphous carbon and the nanotubes defects for larger treatment times (Lafi *et al*. 2005; Li *et al*. 2004).

3.1.3. TGA analysis

Figure 4 displays the TGA results for the SWCNT samples studied, as well as the plot of the first derivative of the TGA data (DTG). The DTG curve for the as-produced nanotubes exhibits two peaks corresponding to the burning-off of two different types of carbon. Previous studies have reported that the peak at 623 K is attributed to the burning of amorphous carbon, whereas the peak at the highest temperature is due to the burning of carbon nanotubes (Harutyunyan *et al*. 2002). The TGA data also show that 30% of the sample mass remained at 1273 K, with this amount corresponding to catalyst impurities. The oxidized samples exhibited higher combustion temperatures than the as-produced sample NT, which can be explained by two factors as follows. Firstly, the amount of catalyst decreased as a result of acid treatment, but the catalyst itself can act

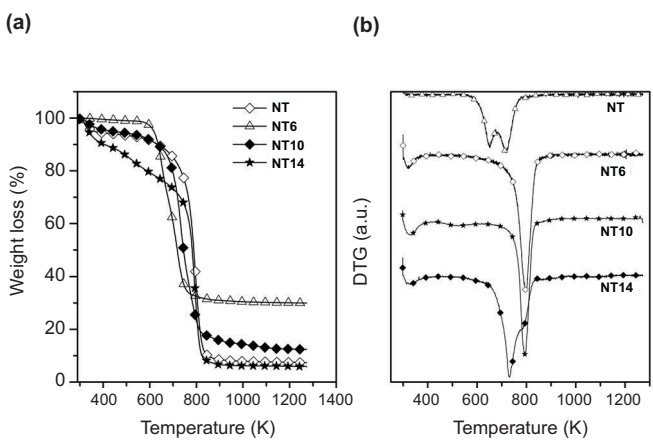

Figure 4. (a) TGA and (b) DTG curves of the SWCNT samples studied.

as an oxidative source (Harutyunyan *et al*. 2002) thereby aiding the combustion process. Secondly, the formation of a more dense and organized structure with less open spaces for the treated samples (as observed in the SEM micrographs) provided greater stability to the carbon nanotubes against oxidation (Kim *et al*. 2008). The NT6 and NT10 samples showed a strong decrease in the mass remaining at 1273 K (ca. 6%), indicating that acid treatment effectively leached out the excess catalyst present in the as-produced nanotubes. The NT6 sample showed only one DTG peak related to the combustion of the nanotubes. This single peak appeared at higher temperatures than the as-produced nanotubes, indicating a higher stability in the NT6 sample. The NT10 sample showed a similar behaviour to the NT6 sample but possessed a significant amount of material which was easily degradable at low temperatures, as revealed by mass loss and the DTG plot. The residual percentage mass at 1273 K for the NT14 sample was slightly higher than those for the NT6 and NT10 samples. On the other hand, the NT14 sample displayed a new and intense DTG peak at ca. 720 K. The presence of this peak indicates that treatment of the nanotubes for 14 h led to the degradation of much more material, perhaps with a significant carbon loss. This decrease in the amount of carbon is probably the reason for the relatively higher percentage of catalyst remaining at 1273 K. The small peak in the DTG plot at 800 K corresponds to the nanotubes present in this sample.

3.1.4. FT-IR analysis

Figure 5 shows the FT-IR spectra which were measured in order to study the evolution of surface functional groups in the samples. The IR spectra are shown over the wavelength range between 900 $cm^{-1}$and 2400 cm^{-1}, where most of the IR bands corresponding to oxygen-containing surface functional groups on carbon surfaces are located (Kim *et al*. 2005; Mawhinney *et al*. 2000; Fuente *et al*. 2003).

For the samples under consideration, changes in the surface groups containing oxygen occurred as the acid-treatment time increased. The NT sample exhibited an important band at ca. 1080 cm^{-1} which may be attributed to the C–O stretching modes in ethers, esters, alcohols or phenolic compounds (Kim *et al*. 2005). This intense band in the spectrum of the NT sample can be attributed to the presence of surface groups containing oxygen in the amorphous carbon. This explains the

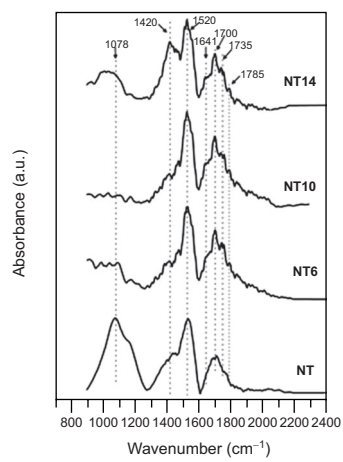

Figure 5. FT-IR spectra of the SWCNT samples studied showing the evolution of surface functional groups.

disappearance of the band in the spectra of the samples treated for 6 h and 10 h. The band appears once more in the spectrum of the sample exposed to longer treatment times (NT14) and may be assigned to functional groups present in the amorphous carbon derived from degraded nanotubes.

The band at 1420 cm^{-1} can be assigned to C–O–H deformation with simultaneous vibration of the C=C bonds corresponding to carboxylic groups (Fuente *et al*. 2003). This band is intense in the spectrum of the NT14 sample, suggesting that this sample had the highest content of carboxylic groups. The band was not appreciable in the spectrum of the NT sample and was of low intensity in the corresponding spectra of the NT6 and NT10 samples.

The absorptions over the wavenumber range 1550–1600 cm^{-1} can be assigned to C=C stretching in the conjugated rings of sp^2 carbons (Fuente *et al*. 2003). This can be considered as a fundamental SWCNT mode (Kim *et al*. 2005) and explains why no changes were observed in the 1520 cm^{-1} band with extended acid treatment.

The bands between 1640 cm^{-1} and 1750 cm^{-1} are attributed to C=O stretching of carbonyl groups. The bands shifted to lower frequencies (1641 cm^{-1}) can be assigned to the stretching of weakly coupled carbonyl groups, for example in quinones located preferentially at the ends of the tubes (Kim *et al*. 2005; Mawhinney *et al*. 2000). The bands shifted to higher frequencies (1735 cm^{-1} and 1786 cm^{-1}) can be attributed to carbonyl groups in carboxylic acids or esters (Fuente *et al*. 2003; Kim *et al*. 2005). As can be observed from Figure 5, oxidation treatment led to an increase in the number of bands in this spectral region, especially those at 1641, 1735 and 1786 cm^{-1}. This indicates that the oxidation treatment led to the development of quinone and carboxylic groups in the oxidized samples, with longer times leading to the development of a greater number of oxidized functional groups, e.g. carboxylic groups in the NT14 sample.

3.1.5. XPS analysis

The XPS spectra depicted in Figure 6 overleaf show the peaks corresponding to the carbon signal, with the prominent peak at 284.5 eV corresponding to the sp^2 carbons of the graphene sheets. The peaks at 285.8, 287.0 and 289.6 eV correspond to –C–O, >C=O and –COO groups, respectively (Kim *et al*. 2008; Xia *et al*. 2007). This figure shows the relative percentage decrease in the peak area corresponding to sp^2 carbon (on the right) and the percentage increase in the peak area of the carbons attached to oxygen (on the left) as a function of the acid-treatment time. The changes in these percentages correspond to the formation of surface oxygen groups on the SWCNTs and its increase with increasing acid-treatment time. These results are in agreement with the FT-IR data and show that acid treatment led to an increase in the number of surface groups containing oxygen in the SWCNTs.

3.1.6. Nitrogen adsorption isotherms

Figure 7 overleaf shows the nitrogen adsorption/desorption isotherms measured at 77 K for the samples under study. In this figure, the volume of nitrogen adsorbed under standard temperature and pressure conditions (STP) per sample mass unit is represented as a function of the relative pressure (P/P_0), where P is the equilibrium pressure and P_0 is the saturation pressure of the adsorbate at 77 K. For the NT sample, adsorption increased significantly at low relative pressures; this was followed by a smooth and more gradual growth in the region where the monolayer ends and the multilayer begins, with a steep increase in coverage occurring as P_0 was approached. The behaviour near P_0 can be associated to the condensation of nitrogen in the spaces amongst the tangled bundles of nanotubes. A large number of adjacent sites can lead to the formation of macropores, as shown in the SEM micrographs (see Figure 2). This behaviour was different for

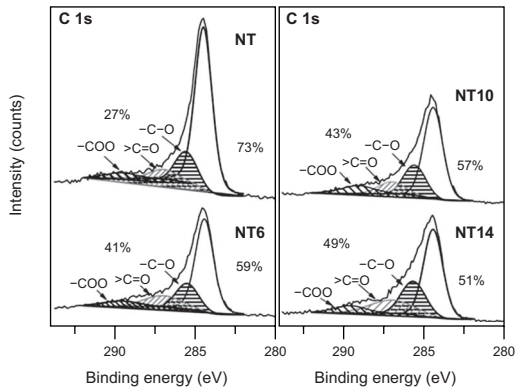

Figure 6. XPS spectra associated with the signal corresponding to carbon for the SWCNT samples studied. The shaded portions correspond to the contributions due to carbon bonded to oxygen. The percentage of the area corresponding to sp^2 carbon is shown on the right-hand side of the peaks; the percentage corresponding to oxygen-bonded carbon is shown to the left of the peak

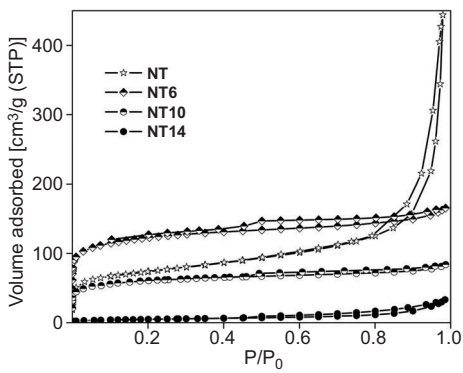

Figure 7. Nitrogen adsorption/desorption isotherms at 77 K for the SWCNT samples studied

the oxidized materials, possibly due to nanotube densification as a result of this treatment removing the spacing between the bundles, as reported by Yang *et al*. (2005).

Table 2 lists the textural properties calculated from the nitrogen adsorption isotherms measured at 77 K. The micropore volume, V_0–N_2, was calculated using the Dubinin–Raduschkevich equation (Dubinin 1960) and compared with the micropore volume calculated from the NLDFT model, showing agreement between the two methods.

In the low relative pressure region, the adsorption isotherm for sample NT6 exhibited typical Type I behaviour according to the BDDT (Brunauer, Deming, Deming and Teller) classification, characteristic of solids with high adsorbate–adsorbent interactions (Brunauer *et al*. 1940). Figure 7 shows that, in the low relative pressure region, the adsorbed volume for sample NT6 was nearly twice that for the as-produced nanotubes. This is reflected in the large increase in the specific surface area (S_{BET}) and micropore volume (V_0) listed in Table 2. This significant increase in the adsorption capacity of the oxidized NT6 sample may be associated with the purification of the as-produced nanotube, i.e. oxidation removes catalyst residues and amorphous carbon. Hence, for

TABLE 2. Specific Surface Area (S_{BET}) and Specific Pore Volumes (V_0–N_2 and V_m) from Nitrogen Adsorption Data at 77 K and Micropore Volume (V_0–CO_2) from Carbon Dioxide Adsorption Data at 273 K for the Various SWCNT Samples Studied

Sample	S_{BET} (m^2/g)	V_0–N_2 (cm^3/g)		V_m[a] (cm^3/g)	V_0–CO_2 (cm^3/g)
		DR	NLDFT		
NT	265	0.11	0.09	0.33	0.08
NT6	510	0.20	0.19	0.07	0.14
NT10	220	0.09	0.08	0.03	0.11
NT14	18	0.01	0.00	0.04	0.06

[a] Mesopore volume computed as the difference between the total pore volume (obtained at a relative pressure of 0.97) and V_0–N_2.

every gram of sample, there is a larger fraction of nanotubes than in the as-produced material. There is no evidence that the increase in amount adsorbed is due to the opening of the ends of the nanotubes; even if they are cut, they remain blocked by the functional groups formed during the cutting process unless an appropriate removal procedure (high-temperature heating under vacuum) is followed (Kuznetsova *et al.* 2000). The NT10 sample exhibited a similar behaviour to the NT6 sample, but a much lower adsorption capacity. This could be associated with the presence of degradable amorphous material at low temperatures (as revealed by TGA), which could block access to some adsorption sites. This fact, and the presence of functional groups generated by the acid treatment, could lead to diffusional problems in the nitrogen adsorption (as discussed below). The NT14 sample had a remarkably low adsorption capacity, probably due to the presence of a larger amount of amorphous material and functional groups. This led to a more extensive blockage of adsorption sites and a significant relative amount of residual catalyst.

The data listed Table 2 also show that the increase in the micropore volume of NT6 sample was followed by a significant decrease in V_0–N_2 with increasing acid-treatment time for samples NT10 and NT14. This is consistent with the previous discussion. It is important to note the significant mesopore volume present in the untreated sample. On applying the NLDFT mode in order to determine the diameter range of these mesopores (not discussed here), it was found that they possessed diameters larger than 200 Å.

Figure 8 overleaf shows plots of the differential pore volume versus pore width (w_p) — commonly called the pore size distribution (PSD) — for the samples studied. It will be seen from the figure that the PSD for the NT sample exhibited a peak in the micropore region at ca. 14 Å. It is notable that the position of the peaks moved towards smaller micropores with increasing acid treatment, thereby suggesting that the NT6 and NT10 samples possessed more energetic sites (probably IC and G sites as shown in Figure 1). The NT14 sample exhibited virtually no microporosity as measured by nitrogen adsorption at 77 K. This may suggest that longer treatment times tended to form condensation regions that decreased or even eliminated the microporosity of the samples.

3.2. Carbon dioxide adsorption isotherms

Nitrogen adsorption studies provide important information on the adsorptive surface and volume characteristics of sorbent materials. However, nitrogen measurements at 77 K are influenced by diffusion problems at this temperature (Garrido *et al.* 1987), whereas CO_2 measurements are not

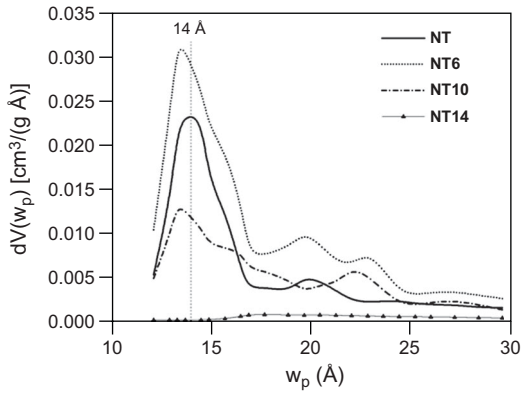

Figure 8. Pore size distributions for the SWCNT samples studied, obtained using the NLDFT method.

affected by such problems due to the higher kinetic energy of the adsorbate molecule at this temperature (Rodríguez-Reinoso and Linares-Solano 1988; Cazorla-Amorós *et al*. 1996). Hence, in order to obtain information on the ultramicropore region (pores smaller than 8 Å) for the samples under study, adsorption studies with CO_2 were conducted (García-Blanco *et al*. 2010). Furthermore, the experiments were carried out at different temperatures in order to calculate the isosteric heats.

The corresponding adsorption isotherm data are shown overleaf in Figure 9. The behaviour of the isotherms as a function of temperature is typical of exothermic processes, viz. the amount adsorbed decreases with increasing temperature. It is important to note that the NT10 sample adsorbed higher volumes of CO_2 than the NT sample, in contrast to the behaviour observed for the adsorption of nitrogen at 77 K.

Since these isotherms have been used to calculate the isosteric heats, it was necessary to ensure the accuracy of these values. Ensuring the correctness of the data required that the sample be adequately degassed and that the equilibration time necessary for the conditions selected be chosen carefully.

Figure 10 below shows the characteristic curves for both N_2 (at 77 K) and CO_2 (at 263, 273, 283 and 289 K) for the different materials under study. The values of the properties used for calculating these curves are listed in Table 3. The CO_2 characteristic curves are linear over all the potential range, indicating that the adsorption of this gas under the studied conditions only occurred in the micropores. In contrast, the nitrogen characteristic curves present (i) deviations at low potential values due to adsorption onto mesopores, (ii) a linear range where micropore filling occurred and (iii) a deviation at higher potential values (narrow micropores), indicating possible diffusional problems. The N_2 and CO_2 characteristic curves of sample NT6 present the same linear trend indicating diffusional problems for N_2 at 77 K in narrow micropores. Otherwise, the N_2 characteristic curves for the NT, NT10 and NT14 samples all display a shift with respect to the corresponding CO_2 curves, this shift being higher for those samples subjected to longer acid-treatment times (samples NT10 and NT14). Hence, it would appear that N_2 diffusional problems at 77 K are generated by the presence of both oxidized functional groups and amorphous carbon.

Table 2 lists the micropore volumes obtained from the CO_2 adsorption data at 273 K (V_0–CO_2) which indicate that the NT10 and NT14 samples exhibited higher micropore volumes than those calculated from N_2 adsorption at 77 K, possibly due to N_2 diffusional problems. This shows the utility of CO_2 in characterizing these kinds of materials.

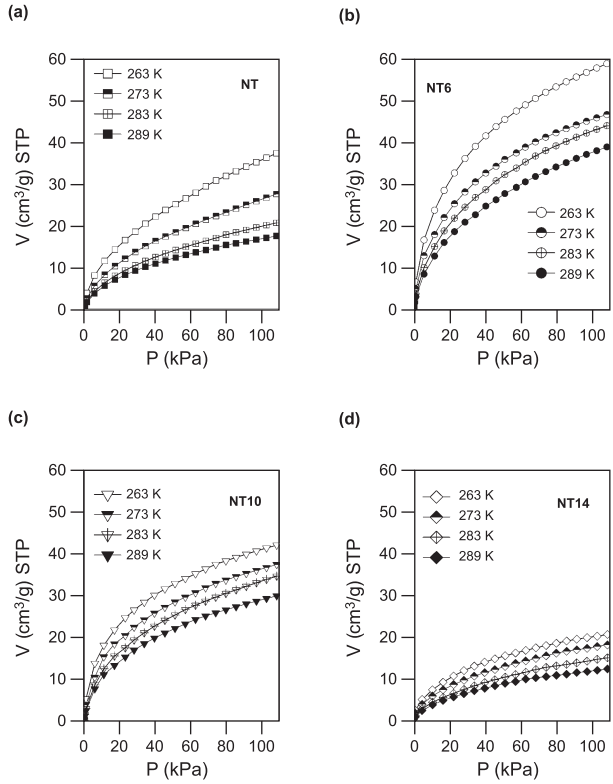

Figure 9. Carbon dioxide adsorption isotherms measured at different temperatures between 263 K and 289 K on the various samples studied: (a) NT; (b) NT6; (c) NT10; (d) NT14.

3.3. Isosteric heats of adsorption

Figure 11 overleaf shows the variation of ln P with respect to 1/T at different values of CO_2 loading onto the NT sample and indicates that the plot displayed good linear behaviour. The other samples studied showed a similar behaviour (not illustrated here). The slopes of the plots depicted in the figure allowed the isosteric heats of adsorption to be determined over the range of adsorbed volumes depicted.

TABLE 3. Nitrogen and Carbon Dioxide Properties Employed in the Calculation of the Characteristic Curves

	T (K)	ρ_s (cm^3/g)	P_0 (kPa)	Ω	β[a]
N_2	77	0.80	–	71.6	0.35
CO_2	263	1.04	2639	91.2	0.44
	273	1.02	3473		
	283	1.00	4488		
	289	0.99	5196		

[a]Obtained using $\Omega_{benzene} = 205.6$.

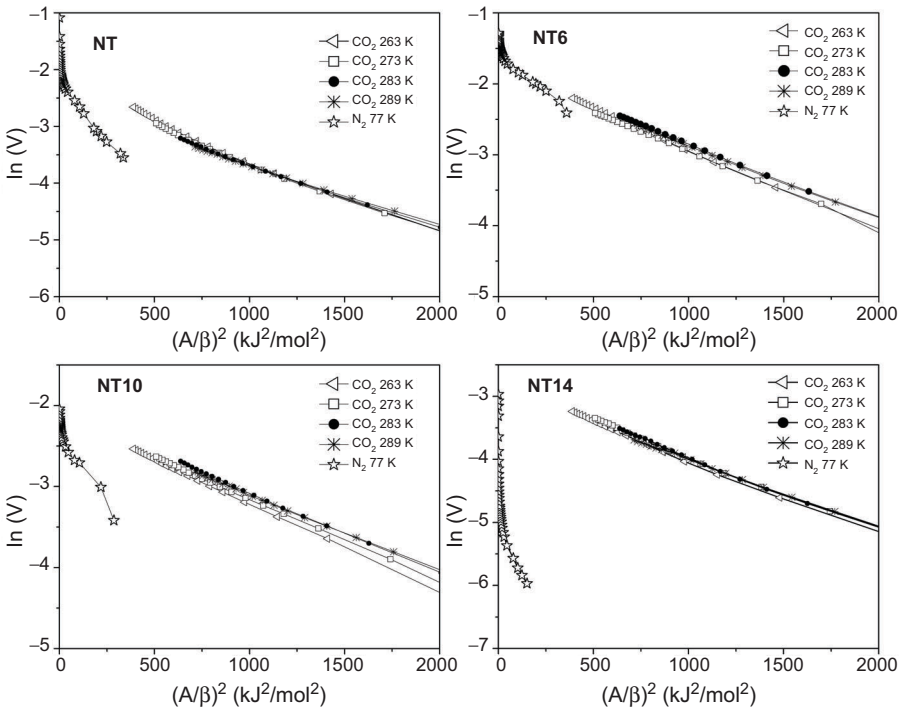

Figure 10. Characteristic curves for the adsorption of nitrogen and carbon dioxide onto the various samples studied.

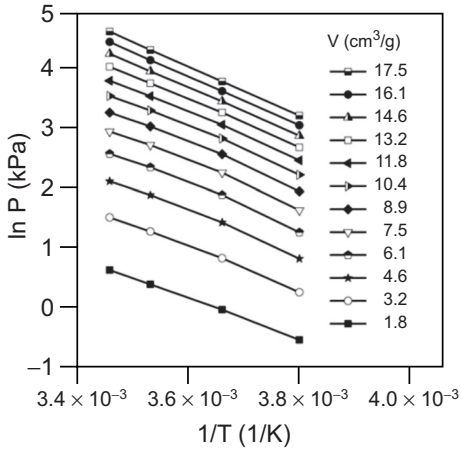

Figure 11. Linear plots of the Napierian logarithm of the pressure, P (kPa), versus 1/T (T in K) for different values of the amounts of CO_2 adsorbed, V (cm^3/g), onto the NT sample.

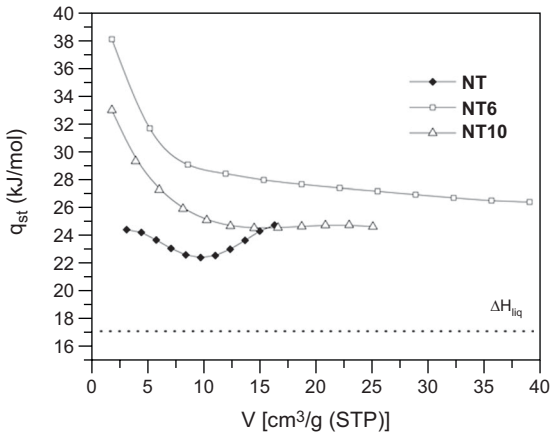

Figure 12. Isosteric heat of adsorption of CO_2, q_{st} (kJ/mol), onto the NT, NT6 and NT10 samples as a function of the amount adsorbed, V [cm^3/g (STP)].

Figure 12 shows the variation of the isosteric heat of adsorption for CO_2 as a function of the quantity adsorbed. The magnitudes of the isosteric heats obtained for the various samples studied indicate that physisorption occurred onto these substrates (Webb and Orr 1997), with the values for the NT sample being in accordance with those measured by Bienfait *et al*. (2004) for SWCNTs at lower loadings. The profiles for the NT6 and NT10 samples indicate that the q_{st} values decreased with loading, indicating a strong adsorbate–adsorbent interaction and a high degree of surface energy heterogeneity (Do 1998; Dunne *et al*. 1996). Such behaviour was not observed with the NT sample. The q_{st} values tend towards the heat of liquefaction (ΔH_{liq}) of CO_2, viz. 17.2 kJ/mol (Bourrelly *et al*. 2005), for all the samples.

As is well known, the CO_2 molecule has a high quadrupole moment (Golden and Sircar 1994), with the presence of such a quadrupole moment being most likely responsible for an increased interaction of CO_2 with any surface oxygen groups present. Thus, in the acid-treated samples, the increase in the number of surface oxygen functional groups would increase the affinity towards CO_2 and may enhance the isosteric heat of adsorption. Consequently, in the analysis of the isosteric heat profiles, it is necessary to take into account both the adsorptive sites of the nanotubes and the interaction with surface functional groups.

4. CONCLUSIONS

The characteristics of single wall carbon nanotube samples treated with nitric acid for different time periods (including the as-prepared sample) have been studied. It has been shown that such acid treatment led to the removal of excess catalytic particles, thereby decreasing the spacing between the bundles, creating a denser and more stable structure, and increasing the number of surface oxygen-containing functional groups. It was also observed that no destruction of the carbon nanotubes occurred on acid treatment up to 6 h, whereas after acid treatment for 10 h and 14 h degradation of the small diameter nanotubes occurred. At the maximum treatment time, the formation of amorphous carbon was evident.

Studies of the adsorption properties indicated that the mesoporosity in the as-produced sample disappeared as a result of acid treatment, with microporosity being generated in the various treated samples which increased in magnitude with acid-treatment time. However, the volume adsorbed in the narrow micropores increased for an acid-treatment time of 6 h, in contrast to the adsorbed volume in the samples treated for 10 h and 14 h, respectively. Diffusional problems in nitrogen adsorption at 77 K were found to occur mainly in those samples subjected to longer oxidation times. Such problems were not observed for the CO_2 adsorption isotherms at the different temperatures under study, thereby showing the utility of this gas in the characterization of the microporosity of SWCNTs. Furthermore, the isosteric heats of adsorption showed that there was strong interaction between CO_2 and the oxidized samples. This strong interaction may be related to the quadrupole moment of the CO_2 molecule.

ACKNOWLEDGMENTS

The authors wish to thank Aldo Migone for supplying the samples studied and for various discussions regarding some of the results obtained in this work. This work was supported financially by UNSL, FONCYT and CONICET (Argentina).

REFERENCES

Albesa, A.G., Fertitta, E.A. and Vicente, J.L. (2010) *Langmuir* **26,** 786.
Ansón, A., Callejas, M.A., Benito, A.M., Maser, W.K., Izquierdo, M.T., Rubio, B., Jagiello, J., Thommes, M., Parra, J.B. and Martínez, M.T. (2004) *Carbon* **42,** 1243.
Baughman, R.H., Zakhidov, A.A. and de Heer, W.A. (2002) *Science* **297,** 787.
Bienfait, M., Zeppenfeld, P., Dupont-Pavlovsky, N., Muris, M., Johnson, M.R., Wilson, T., DePies, M. and Vilches, O.E. (2004) *Phys. Rev. B* **70,** 035410-1.
Bourrelly, S., Llewellyn, P.L., Serre, C., Millange, F., Loiseau, T. and Férey, G. (2005) *J. Am. Chem. Soc.* **127,** 13519.
Brunauer, S., Deming, L.S., Deming, W.E. and Teller, E. (1940) *J. Am. Chem. Soc.* **62**, 1723.
Calbi, M.M., Gatica, S.M., Bojan, M.J. and Cole, M.W. (2001) *J. Chem. Phys.* **115,** 9975.
Cao, D., Zhang, X., Chen, J., Wang, W. and Yun, J. (2003) *J. Phys. Chem. B* **107**, 13286.
Cazorla-Amorós, D., Alcañiz-Monge, J. and Linares-Solano, A. (1996) *Langmuir* **12,** 2820.
Chen, W., Fan, Z., Pan, X. and Bao, X. (2008) *J. Am. Chem. Soc.* **130,** 9414.
Cinke, M., Li, J., Bauschlicher Jr., C.W., Ricca, A. and Meyyappan, M. (2003) *Chem. Phys. Lett.* **376,** 761.
Cruz, F.J.A.L., Esteves, I.A.A.C. and Mota, J.P.B. (2010) *Colloids Surf. A* **357,** 43.
Dai, H. (2002) *Surf. Sci.* **500,** 218.
Dillon, A.C., Jones, K.M., Bekkedahl, T.A., Kiang, C.H., Bethune, D.S. and Heben, M.J. (1997) *Nature (London)* **386,** 377.
Do, D.D. (1998) *Adsorption Analysis: Equilibria and Kinetics*, Imperial College Press, London, U.K.
Dresselhaus, M.S., Dresselhaus, G., Saito, R. and Jorio, A. (2005) *Phys. Rep.* **409,** 47.
Dubinin, M.M. (1960) *Chem. Rev.* **60,** 235.
Dunne, J.A., Mariwala, R., Rao, M., Sircar, S., Gorte, R.J. and Myers, A.L. (1996) *Langmuir* **12,** 5888.
Esteves, I.A.A.C., Cruz, F.J.A.L., Müller, E.A., Agnihotri, S. and Mota, J.P.B. (2009) *Carbon* **47,** 948.
Eswaramoorthy, M., Sen, R. and Rao, C.N.R. (1999) *Chem. Phys. Lett.* **304,** 207.
Fuente, E., Menéndez, J.A., Díez, M.A., Suárez, D., and Montes-Morán, M.A. (2003) *J. Phys. Chem. B* **107**, 6350.

Furmaniak, S., Terzyk, A.P., Gauden, P.A. and Rychlicki, G. (2006) *J. Colloid Interface Sci.* **295,** 310.
García Blanco, A.A., Alexandre de Oliveira, J.C., López, R., Moreno-Piraján, J.C., Giraldo, L., Zgrablich, G. and Sapag, K. (2010) *Colloids Surf. A* **357,** 74.
Garrido, J., Linares-Solano, A., Martín-Martínez, J.M., Molina-Sabio, M., Rodríguez-Reinoso, F. and Torregrosa, R. (1987) *Langmuir* **3,** 76.
Golden, T.C. and Sircar, S. (1994) *J. Colloid Interface Sci.* **162,** 182.
Graham, U.M., Dozier, A., Khatri, R.A., Bahome, M.C., Jewell, L.L., Mhlanga, S.D., Coville, N.J. and Davis, B.H. (2009) *Catal. Lett.* **129,** 39.
Harutyunyan, A.R., Pradhan, B.K., Chang, J., Chen, G. and Eklund, P.C. (2002) *J. Phys. Chem. B* **106,** 8671.
Hu, H., Zhao, B., Itkis, M.E. and Haddon, R.C. (2003) *J. Phys. Chem. B* **107,** 13838.
Iijima, S. (1991) *Nature (London)* **354,** 56.
Itkis, M.E., Perea, D.E., Niyogi, S., Rickard, S.M., Hamon, M.A., Hu, H., Zhao, B. and Haddon, R.C. (2003) *Nano Lett.* **3,** 309.
Kataura, H., Kumazawa, Y., Maniwa, Y., Ohtsuka, Y., Sen, R., Suzuki, S. and Achiba, Y. (2000) *Carbon* **38,** 1691.
Kim, D.Y., Yang, C.-M., Noguchi, H., Yamamoto, M., Ohba, T., Kanoh, H. and Kaneko, K. (2008) *Carbon* **46,** 611.
Kim, U.J., Furtado, C.A., Liu, X., Chen, G. and Eklund, P.C. (2005) *J. Am. Chem. Soc.* **127,** 15437.
Krungleviciute, V., Heroux, L., Talapatra, S. and Migone, A.D. (2004) *Nano Lett.* **4,** 1133.
Kuznetsova, A., Mawhinney, D.B., Naumenko, V., Yates Jr., J.T., Liu, J. and Smalley, R.E. (2000) *Chem. Phys. Lett.* **321,** 292.
Lafi, L., Cossement, D. and Chahine, R. (2005) *Carbon* **43,** 1347.
Lee, S.M., Park, K.S., Choi, Y.C., Park, Y.S., Bok, J.M., Bae, D.J., Nahm, K.S., Choi, Y.G., Yu, S.C., Kim, N.G., Frauenheim, T. and Lee, Y.H. (2000) *Synth. Met.* **113,** 209.
Li, Y., Zhang, X., Luo, J., Huang, W., Cheng, J., Luo, Z., Li, T., Liu, F., Xu, G., Ke, X., Li, L. and Geise, H.J. (2004) *Nanotechnology* **15,** 1645.
Lu, C., Bai, H., Wu, B., Su, F. and Hwang, J.F. (2008) *Energy Fuels* **22,** 3050.
Mawhinney, D.B., Naumenko, V., Kusnetsova, A., Yates, J.T., Liu, J. and Smalley, R.E. (2000) *J. Am. Chem. Soc.* **122,** 2383.
Migone, A.D. and Talapatra, S. (2004) "Adsorption Studies on Carbon Nanotubes", in *Encyclopedia of Nanoscience and Nanotechnology*, Vol. 4, Nalwa, H.S., Ed, American Scientific Publishers, Los Angeles, CA, U.S.A., p. 749.
Ohba, T. and Kaneko, K. (2002) *J. Phys. Chem. B* **106,** 7171.
Panella, B., Hirscher, M. and Roth, S. (2005) *Carbon* **43,** 2209.
Polanyi, M. (1914) *Verh. Dtsch. Phys. Ges.* **16,** 1012.
Quayle, O.R. (1953) *Chem. Rev.* **53,** 439.
Rawat, D.S., Krungleviciute, V., Heroux, L., Bulut, M., Calbi, M.M. and Migone, A.D. (2008) *Langmuir* **24,** 13465.
Reid, R.C., Prausnitz, J.M. and Poling, B.E. (1987) *The Properties of Gases and Liquids*, 4th Edn, McGraw-Hill, New York.
Rodríguez-Reinoso, F. and Linares-Solano, A. (1988) *Chem. Phys. Carbon* **21,** 36.
Ruthven, D.M. (1984) *Principles of Adsorption and Adsorption Processes*, John Wiley & Sons, New York.
Rzepka, M., Lamp, P. and de la Casa-Lillo, M.A. (1998) *J. Phys. Chem. B* **102,** 10894.
Satterfield, C.N. (1993) *Heterogeneous Catalysis in Industrial Practice*, 2nd Edn, McGraw-Hill, New York.
Serp, P., Corrias, M. and Kalck, P. (2003) *Appl. Catal. A* **253,** 337.
Simonyan, V.V. and Johnson, J.K. (2002) *J. Alloy Compd.* **330–332,** 659.
Sircar, S. (1991) *Langmuir* **7,** 3065.
Spencer C.F. and Danner, R.P. (1972) *J. Chem. Eng. Data* **17,** 236.
Szekely, J., Evans, J.W. and Sohn, H.Y. (1976) *Gas–Solid Reactions*, Academic Press, New York.
Talapatra, S. and Migone, A.D. (2001) *Phys. Rev. Lett.* **87,** 206106-1.

Wagner, W. (1973) *Cryogenics* **13,** 470.
Webb, P.A. and Orr, C. (1997) *Analytical Methods in Fine Particle Technology*, Micromeritics Instrument Corporation, Norcross, GA, U.S.A.
Wood, G.O. (2001) *Carbon* **39,** 343.
Xia, W., Wang, Y., Bergsträβer, R., Kundu, S. and Muhler, M. (2007) *Appl. Surf. Sci.* **254,** 247.
Yang, C.-M., Kanoh, H., Kaneko, K., Yudasaka, M. and Iijima, S. (2002) *J. Phys. Chem. B* **106,** 8994.
Yang, C.-M., Kim, D.Y. and Lee, Y.H. (2005) *Chem. Mater.* **17,** 6422.
Yin, S.F., Xu, B.Q., Zhu, W.X., Ng, C.F., Zhou, X.P. and Au, C.T. (2004) *Catal. Today* **93–95,** 27.
Zhou, Y., Feng, K., Sun, Y. and Zhou, L. (2003) *Chem. Phys. Lett.* **380,** 526.